

## JGR Atmospheres

## RESEARCH ARTICLE

10.1029/2020JD032863

## Snowfall and Water Stable Isotope Variability in East Antarctica Controlled by Warm Synoptic Events

## Key Points:

- Specific conditions associated with large snowfall events on East Antarctic Plateau cause a bias in temperature during precipitation
- Water stable isotopes in snow record atmospheric conditions during precipitation

## Supporting Information:

- Supporting Information S1
- Table S1

## Correspondence to:

A. P. M. Servettaz,  
aymeric.servettaz@gmail.com

## Citation:

Servettaz, A. P. M., Orsi, A. J., Curran, M. A. J., Moy, A. D., Landais, A., Agosta, C., et al. (2020). Snowfall and water stable isotope variability in East Antarctica controlled by warm synoptic events. *Journal of Geophysical Research: Atmospheres*, 125, e2020JD032863. <https://doi.org/10.1029/2020JD032863>

Received 1 APR 2020

Accepted 2 AUG 2020

Accepted article online 6 AUG 2020

## Author Contributions:

**Conceptualization:** Aymeric P. M. Servettaz, Anais J. Orsi

**Data curation:** Mark A. J. Curran, Andrew D. Moy, V. Holly L. Winton, Alexandra Touzeau, Joseph R. McConnell, Mélanie Baroni

**Formal analysis:** Aymeric P. M. Servettaz, Anais J. Orsi

**Funding acquisition:** Anais J. Orsi, Mark A. J. Curran, Amaelle Landais

**Investigation:** Aymeric P. M. Servettaz, V. Holly L. Winton, Alexandra Touzeau

**Methodology:** Aymeric P. M. Servettaz, Anais J. Orsi











**Project administration:** Mark A. J. Curran

**Resources:** Cécile Agosta, Martin Werner

**Software:** Cécile Agosta, Martin Werner

**Supervision:** Anais J. Orsi, Mark A. J. Curran

(continued)

Aymeric P. M. Servettaz<sup>1</sup> , Anais J. Orsi<sup>1</sup> , Mark A. J. Curran<sup>2,3</sup>, Andrew D. Moy<sup>2,3</sup> , Amaelle Landais<sup>1</sup> , Cécile Agosta<sup>1</sup> , V. Holly L. Winton<sup>4,5</sup> , Alexandra Touzeau<sup>6</sup> , Joseph R. McConnell<sup>7</sup> , Martin Werner<sup>8</sup> , and Mélanie Baroni<sup>9</sup> 

<sup>1</sup>Laboratoire des Sciences du Climat et de l'Environnement, LSCE/IPSL, CEA-CNRS-UVSQ, Université Paris-Saclay, Gif-sur-Yvette, France, <sup>2</sup>Australian Antarctic Division, Kingston, Tasmania, Australia, <sup>3</sup>Antarctic Climate and Ecosystems Cooperative Research Centre, University of Tasmania, Hobart, Tasmania, Australia, <sup>4</sup>Physics and Astronomy, Curtin University, Perth, Western Australia, Australia, <sup>5</sup>Antarctic Research Centre, Victoria University of Wellington, Wellington, New Zealand, <sup>6</sup>Geophysical Institute and Bjerknes Centre for Climate Research, University of Bergen, Bergen, Norway, <sup>7</sup>Division of Hydrologic Sciences, Desert Research Institute, Reno, NV, USA, <sup>8</sup>Helmholtz Centre for Polar and Marine Research, Alfred Wegener Institute, Bremerhaven, Germany, <sup>9</sup>Centre Européen de Recherche et d'Enseignement des Géosciences de l'Environnement, Université Aix-Marseille, Aix-en-Provence, France

**Abstract** Understanding climate proxy records that preserve physical characteristics of past climate is a prerequisite to reconstruct long-term climatic conditions. Water stable isotope ratios ( $\delta^{18}\text{O}$ ) constitute a widely used proxy in ice cores to reconstruct temperature and climate. However, the original climate signal is altered between the formation of precipitation and the ice, especially in low-accumulation areas such as the East Antarctic Plateau. Atmospheric conditions under which the isotopic signal is acquired at Aurora Basin North (ABN), East Antarctica, are characterized with the regional atmospheric model Modèle Atmosphérique Régional (MAR). The model shows that 50% of the snow is accumulated in less than 24 days year<sup>-1</sup>. Snowfall occurs throughout the year and intensifies during winter, with 64% of total accumulation between April and September, leading to a cold bias of  $-0.86^\circ\text{C}$  in temperatures above inversion compared to the annual mean of  $-29.7^\circ\text{C}$ . Large snowfall events are associated with high-pressure systems forcing warm oceanic air masses toward the Antarctic interior, which causes a warm bias of  $+2.83^\circ\text{C}$ . The temperature- $\delta^{18}\text{O}$  relationship, assessed with the global atmospheric model ECHAM5-wiso, is primarily constrained by the winter variability, but the observed slope is valid year-round. Three snow  $\delta^{18}\text{O}$  records covering 2004–2014 indicate that the anomalies recorded in the ice core are attributable to the occurrence of warm winter storms bringing precipitation to ABN and support the interpretation of  $\delta^{18}\text{O}$  in this region as a marker of temperature changes related to large-scale atmospheric conditions, particularly blocking events and variations in the Southern Annular Mode.

## 1. Introduction

Understanding the climate of Antarctica is essential for the interpretation of ice cores. The calibration of proxy records during the instrumental period allows us to interpret ice-core records over the last few millennia or under conditions similar to present day, when the calibration has been made. Recent climate is known from meteorological observations and extensive snow studies that overlap with satellite era data since 1979 (Fogt et al., 2017). Given the brevity and sparsity of observational data, it remains difficult to assess the climate variability and trends in Antarctica (Jones et al., 2016) at decadal and longer timescales. Paleoclimate data such as ice-core records help to evaluate changes in atmospheric conditions over longer timescales, with the assumption that we understand how climate information is expressed in the climate proxy.

Ice cores provide a variety of proxy records that can be used to reconstruct past climatic conditions. One of these proxies, water isotope ratio in snow and ice, can be used to trace past temperatures. The isotope ratios of oxygen and hydrogen scale with temperature due to preferential removal of heavy isotopes by the partial precipitation of water in the air masses when they move poleward and cool down (Dansgaard, 1964; Jouzel & Merlivat, 1984; Masson-Delmotte et al., 2008). The most common water isotope ratios are given relative to standard mean ocean water and noted  $\delta^{18}\text{O}$  and  $\delta\text{D}$  (Craig, 1961; Dansgaard, 1964). In Antarctica, water isotopes have been widely used in ice cores across the continent to infer past temperatures (Jouzel, 2003; Stenni

**Validation:** Anais J. Orsi, Mark A. J. Curran, Amaelle Landais, Cécile Agosta

**Writing - original draft:** Aymeric P. M. Servettaz

**Writing - review & editing:** Aymeric P. M. Servettaz, Anais J. Orsi, Mark A. J. Curran, Andrew D. Moy, Amaelle Landais, Cécile Agosta, V. Holly L. Winton, Alexandra Touzeau, Joseph R. McConnell, Martin Werner, Mélanie Baroni

et al., 2017), with the oldest continuous ice core drilled to this day dating back to 800,000 years before 1950 (EPICA community members, 2004).

Advances in analytical methods and introduction of Cavity Ring-Down Spectroscopy have allowed precise measurements of  $\delta^{18}\text{O}$  and  $\delta\text{D}$  with a decreased analysis time, leading to a substantial increase in resolution (Gupta et al., 2009). However, archival limitations due to intermittency of precipitation events and loss of short periodicity signal due to postdeposition processes are particularly important in low-accumulation areas, such as the East Antarctic Plateau (Casado et al., 2018, 2019). Deep ice cores drilled on the East Antarctic Plateau provide climate information over long timescales with a low (>50 year) resolution, complementing the short instrumental record (Ekaykin et al., 2017). Decadal to centennial variability, however, is not fully understood, although it is of increasing interest for secular projections (Jones et al., 2016). While coastal ice cores have a much higher resolution, they often record oceanic signals such as changes in sea ice conditions (Bertler et al., 2011, 2018; Rhodes et al., 2012; Thomas et al., 2019) and are not representative of the continental landmass (Altnau et al., 2015). This gap of data could benefit from ice cores drilled in higher accumulation areas on the plateau's edges, such as the recently drilled Aurora Basin North (ABN) ice core, with the aim clarifying the last 2,000 years of climate variability in East Antarctica. To this end, we seek to investigate how stable isotopes of water at this ice-core site track climate variability.

To understand the climate record at the ABN drilling site, we study how precipitation events affected the snow and ice water isotope record at a site where snow precipitation is lower than coastal sites but is higher compared to ice-core sites on the Antarctic Plateau. First, we use the polar-oriented regional climate model *Modèle Atmosphérique Régional* (MAR) which performs well in Antarctica (Agosta et al., 2019) to describe the precipitation climatology and estimate the biases due to (1) seasonality and (2) warming associated with the air masses responsible for precipitation. We investigate the regional significance of ABN climate and the conditions in which precipitation events occur. We discuss possible implication for other east Antarctic Plateau sites where the precipitation mechanisms are similar. Then, we assess how climate information is passed to  $\delta^{18}\text{O}$  using the isotope-enabled model ECHAM5-wiso (Werner et al., 2011), which is suited for isotope studies in Antarctica (e.g., Goursaud et al., 2018). Finally, we demonstrate that season-long anomalies are recorded in the  $\delta^{18}\text{O}$  by comparing the modeled temperature and atmospheric modes with high-resolution snow pit isotope measurements.

## 2. Material and Methods

### 2.1. Site and Sample Description

ABN (71.17°S, 111.37°E at 2,690-m elevation) is the site selected for the single summer drilling campaign conducted in the 2013–2014 season by the Australian Antarctic Science Program. The drilling site is located on the lower elevation edge of the East Antarctic Plateau, ~500 km inland of the coastal station Casey, approximately halfway to Concordia station on Dome C (Figure 1).

Samples for water isotopes ( $\delta\text{D}$  and  $\delta^{18}\text{O}$ ) analysis include the following: a shallow 12-m firn core analyzed on a Picarro L2130-i isotopic water analyzer using a continuous flow analysis (CFA), melt system at Desert Research Institute, Reno, Nevada (Maselli et al., 2013; McConnell et al., 2002), and discrete snow samples were collected from two parallel profiles in a 2.5-m deep snow pit located in a designed clean area ~1 km from the main camp. Sampling took place between 7 and 9 January 2014. One profile of the snow pit was analyzed by the Australian Antarctic Division (AAD) at 2.5-cm resolution on a Picarro L2130-i isotopic water analyzer, and the other was analyzed at Laboratoire des Sciences du Climat et de l'Environnement (LSCE) at a 3-cm resolution on a Picarro L2130-i. Isotopic values are expressed as per mil (‰) and relative to the Vienna Standard Mean Oceanic Water (V-SMOW) standard. The standard deviation for repeated measurements of laboratory reference water samples was less than 0.05‰ for  $\delta^{18}\text{O}$  and less than 0.5‰ for  $\delta\text{D}$  for this series of measurements.

Annual surface temperature from the nearby automatic weather station GC41 (71.60°S, 111.26°E, operation period 1985–1992) averages  $-43.7^\circ\text{C}$ . This value is consistent with the borehole temperature measured at ABN, of  $-43.4 \pm 0.3^\circ\text{C}$  (with three measures downward and three measures upward from 16.5 to 31.5 m), although this value needs to be taken with caution because the temperature was measured shortly after the core was drilled.

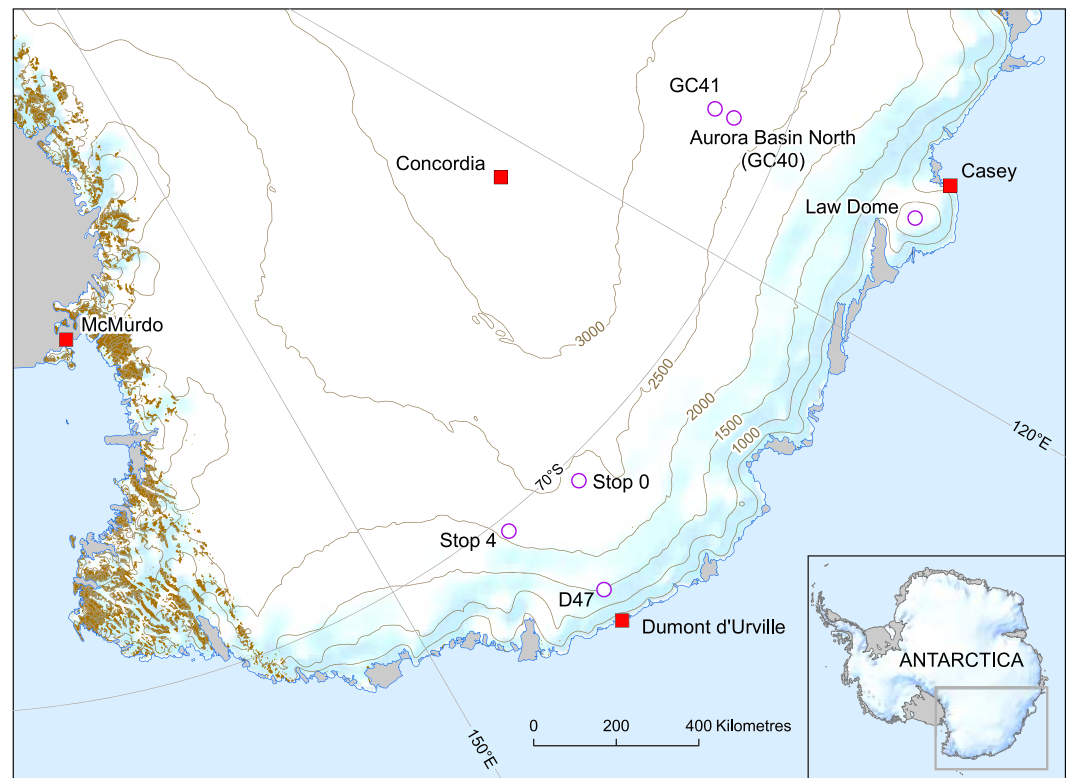


**Figure 1.** Map of the Aurora Basin North site and a selection of Antarctic stations and coring locations. Adapted from a production of the Australian Antarctic Data Centre, September 2013 (map catalogue no. 14254—data.aad.gov.au © Commonwealth of Australia 2013).

Snow pits and the short core were dated annually using seasonally varying signal of non-sea-salt sulfur or sulfates (peaking in spring) and sodium (peaking in late winter; Sigl et al., 2016). Yearly horizons were counted up from the sulfur fallout of Pinatubo eruption, which peaked in 1993 in Antarctica (Cole-Dai & Mosley-Thompson, 1999; horizons are shown in Figure S1). Deeper horizons were identified, dating back to 1969. The dating horizons were adjusted within a year for the measured  $\delta^{18}\text{O}$  to provide a better match with the temperature and isotope outputs generated by the models between 1979 and 2014. Two different model fits were assessed: (1) MAR temperature and (2) ECHAM5-wiso  $\delta^{18}\text{O}$ , and both resulted in a similar dating, with a median difference of 1 month and a maximum difference of 4 months. The details of the matching process and comparison of age models are given in the Supporting Information S1 and illustrated by Figures S2–S8.

Based on the dating of the DRI short core and local density measurements, we estimate a mean annual accumulation of 119-mm water equivalent (hereafter abbreviated mm w.eq.) for the 1979–2013 period, with an interannual variability of  $\pm 33$  mm w.eq. ( $1\sigma$ ). Other estimations of accumulation from the snow pits are shown in Table S1. Postdeposition mixing of snow and surface topography features were observed on site and might affect the top ~10 cm of snow (up to 40 mm w.eq.). The dating uncertainty due to surface roughness is thus estimated to  $\pm 4$  months.

## 2.2. Models

### 2.2.1. The Regional Climate Model MAR

To assess the climate at ABN, which is hundreds of kilometers away from the nearest permanent meteorological station, we use the regional atmospheric climate model MAR nudged to ERA-Interim climate reanalysis (European Centre for Medium-Range Weather Forecast reanalysis interim data set; Dee et al., 2011). The model simulation with MAR for Antarctica covering the period 1979–2015 was performed and evaluated by Agosta et al. (2019). The MAR model simulations were used as this model was developed with implementation of specific physical parameterizations for polar regions (Agosta

et al., 2019), with a high resolution of  $35 \times 35$  km. The MAR turbulent scheme is adapted for stable conditions of the Antarctic Plateau (Gallée et al., 2015) and has a high vertical resolution near the surface (five levels in the first 10 m above the surface), which enables a better representation of temperature inversion conditions compared to other models. MAR shows a strong correlation with observations ( $r^2 = 0.83$  for all Antarctica) and has low surface mass balance (SMB, defined as precipitation minus evaporation) bias over inland East Antarctica (Agosta et al., 2019). The yearly SMB simulated by MAR at ABN averages 118 mm w.eq. for the 1979–2013 period, with an interannual variability of  $\pm 22$  mm w.eq. ( $1\sigma$ ), in agreement with the estimated accumulation of 119 mm w.eq. Snow drift after deposition is not modeled in MAR, and it is known to significantly affect the SMB of windy areas (Agosta et al., 2019). Because ABN is on the lower elevation edge of the Antarctic Plateau, katabatic winds usually occur, with a mean summer wind speed of  $6.0 \text{ m s}^{-1}$  at 4 m above ground level with prevailing southerly winds (wind speed and direction data availability restricted to summers for 2014–2017, from Automatic Weather Station AuroraBN, [aws.acecrc.org.au/AuroraBN.html](http://aws.acecrc.org.au/AuroraBN.html)). We compare modeled SMB and accumulation from snow records in Table S1.

MAR performs well in simulating the 2-m temperature at the automatic weather station GC41 with a mean bias of  $+0.9^\circ\text{C}$  (for the period 1985–1992), whereas the bias is of  $+4.7^\circ\text{C}$  in ERA-Interim (Figures S9–S11). The warm bias in ERA-Interim is due to an overestimate of the surface turbulent fluxes in very stable conditions (Fréville et al., 2014). The day-to-day temperature variability is also more accurate with MAR than ERA-Interim, yet some low temperatures in winter are not represented fully, causing a slight underestimation of the seasonal range.

### 2.2.2. The Isotope-Enabled General Circulation Model ECHAM5-wiso

The general circulation model ECHAM5-wiso simulates water isotopologues  $\text{H}_2^{16}\text{O}$ ,  $\text{H}_2^{18}\text{O}$ , and  $\text{HD}^{16}\text{O}$ ; hence, it is able to trace  $\delta^{18}\text{O}$  and  $\delta\text{D}$  in water vapor and precipitations (Werner et al., 2011). The use of this model gives a detailed view of how the isotopic signal is recorded in precipitation in response to changes in temperature and atmospheric conditions. We present results of a simulation with a horizontal spatial resolution of  $1.1^\circ \times 1.1^\circ$ , where ECHAM5-wiso has been nudged to ERA-Interim for the period 1979–2015.

ECHAM5-wiso performance in Antarctica has been evaluated by Goursaud et al. (2018) and shows a warm bias on East Antarctic Plateau stations: the computed mean temperature is higher than observations by  $1.1^\circ\text{C}$  at Concordia and by  $4.7^\circ\text{C}$  at GC41, because winter temperatures are not cold enough in the model (Figure S11). There is also a much larger cold bias for coastal stations, with mean temperature at Casey  $7.3^\circ\text{C}$  colder than observed. This is likely due to the coarse resolution of the model that inaccurately represents the steep changing topography of coastal areas. Similarly, mean  $\delta^{18}\text{O}$  is generally higher than observed in the interior and lower on the coast. ECHAM5-wiso underestimates the seasonal temperature range on the plateau. Furthermore, ECHAM5-wiso overestimates the amplitude of  $\delta^{18}\text{O}$  annual cycles (Goursaud et al., 2018) and introduces very light and extremely  $^{18}\text{O}$ -depleted precipitations in winter on the East Antarctic Plateau, which are probably an artifact caused by the calculation of delta values for very low precipitation rates in ECHAM5-wiso model. Therefore, the computed isotope-temperature slope is too large. With all these caveats in mind, we restrict our interpretation of the model output to the study of isotope sensitivity to temperature changes and its link with atmospheric conditions.

## 3. Climatology of the Precipitation in the MAR Model

Ice-core records are not comprised of continuously deposited snow. Rather, the intermittent precipitation causes unevenness of the climate recorded in the ice core. Water stable isotope ratios in precipitation are closely related to condensation temperature (Dansgaard, 1964) and form the parameter that we measure in snow and ice. In order to investigate the ability of water isotopes to record temperature, an understanding of how the isotopic signal is formed and then preserved in precipitation is required. In this section, we demonstrate that extreme precipitation events are overrepresented in deposited snow, and we quantify the associated bias in temperature and seasonality, using outputs from the MAR model nudged to ERA-Interim.



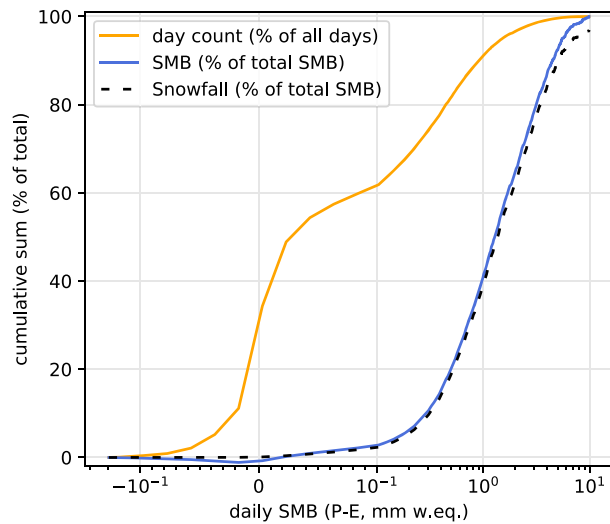


**Figure 2.** Cumulative sum of number of days (orange line), SMB (blue line, defined as precipitation minus evaporation), and snowfall (as percent of total SMB), with days sorted by daily SMB in MAR outputs for ABN site. Note that  $x$ -axis is linear between  $-10^{-1}$  and  $10^{-1}$  mm w.eq.  $\text{day}^{-1}$  and logarithmic outside of this range.

### 3.1. Distribution of Precipitation Events

Snowfall events vary in size and are unevenly distributed throughout the year in Antarctica. Analysis of the distribution of cumulated daily SMB (defined as precipitation minus evaporation) from MAR-ERA-Interim over the 1979–2015 period is investigated at ABN.

Figure 2 shows the cumulative day count, and the cumulative SMB of days, sorted by daily SMB. In the MAR model, daily SMB at ABN ranges from  $-0.2$  to  $+8$  mm w.eq.  $\text{day}^{-1}$  in the 1979–2015 period. About 30% of the days have negative daily SMB (loss of mass), and less than 10% of the days have an accumulation greater than 1 mm w.eq.  $\text{day}^{-1}$ .

We find that the snowfall accounts for 95% of the total SMB while evaporation-condensation processes are responsible for less than 5% of the total SMB, although hoar frost and clear-sky precipitation might be underestimated in the models (Agosta et al., 2019; Stenni et al., 2016). This indicates that precipitation is controlling the SMB record.

Half of the yearly precipitation is deposited during less than 10% of the days, corresponding to 24 days  $\text{year}^{-1}$  on average. This means that the ice is not accumulated evenly throughout a year and will be mostly due to a few large events. Consequently, large precipitation

events significantly bias the recorded signal toward the conditions under which they occur. In the next sections, we analyze the specificities and variability of precipitation events. For simplicity, we distinguish the days with high ( $>1$  mm w.eq.  $\text{day}^{-1}$ ) and low SMB, which represents 58% and 42% of the total SMB, respectively.

### 3.2. Seasonality and Variability of Precipitation

SMB is higher in winter months, with a mean monthly SMB above 11 mm w.eq.  $\text{month}^{-1}$  in May through August (MJJA), compared to 5.8 mm w.eq.  $\text{month}^{-1}$  in December or 7.2 mm w.eq.  $\text{month}^{-1}$  in January (Figure 3a). The winter monthly SMB is variable compared to summer SMB, with interquartile ranges higher than 8 mm w.eq.  $\text{month}^{-1}$  in MJJA compared with 4.5 mm w.eq.  $\text{month}^{-1}$  in December and January. However, if we consider the interquartile range relative to the mean SMB, the variability is constant throughout the year, with highest relative variability in October and November, due to low mean SMB. Slightly more snow is deposited in winter, with 64% of total SMB in April through September, so the winter signal will be enhanced in snowfall-dependent proxies such as water isotopes, which could affect reconstructed temperatures (Persson et al., 2011). That is, if water isotopes were only sensitive to condensation temperature above the site, the annual mean temperature as recorded by the water isotopes in the snow would be  $0.86^\circ\text{C}$  lower than the true annual mean temperature.

The distinction between monthly SMB resulting from low ( $<1$  mm w.eq.  $\text{day}^{-1}$ , white) and high ( $>1$  mm w.eq.  $\text{day}^{-1}$ , blue) daily SMB is shown in Figure 3b. High SMB are characterized by a large spread of monthly means, with interquartile ranges of at least 3.3 and up to 11.1 mm w.eq.  $\text{month}^{-1}$ , twice as large as interquartile ranges of the SMB during small rates that range from 1.5 to 2.7 mm w.eq.  $\text{month}^{-1}$ . This shows that most of the variability in the SMB is due to the large events with high daily precipitation rates. The importance of high-precipitation events on interannual variability of SMB is relevant for most of Antarctica (Turner et al., 2019).

To sum up, low ( $<1$  mm w.eq.  $\text{day}^{-1}$ ) precipitation events happen regularly during the year and provide a baseline of SMB, without specific seasonality. In addition, high-precipitation events can happen throughout the year but with a larger prevalence in winter. These high-precipitation events are responsible for the interannual variability in precipitation (Turner et al., 2019) and drive the seasonal cycle, possibly causing a bias in the distribution of water isotopes in the snow. In the next section, we investigate the meteorological conditions occurring during these high-precipitation events.

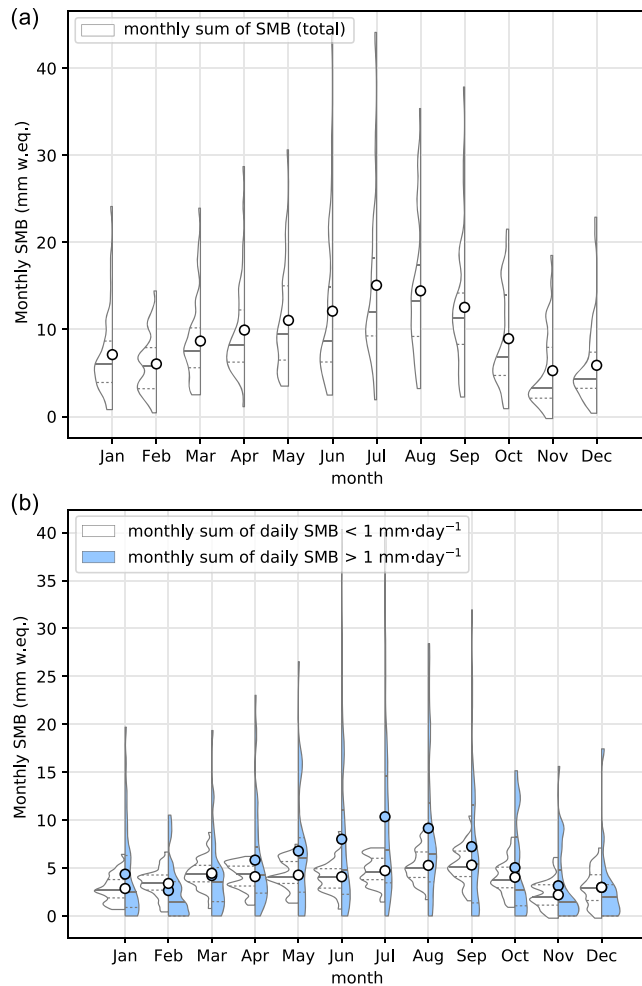


**Figure 3.** Probability density function of (a) monthly SMB, and (b) monthly SMB due to low ( $<1 \text{ mm w.eq. day}^{-1}$ , white) and high ( $>1 \text{ mm w.eq. day}^{-1}$ , blue) daily SMB rates. Mean (colored circles), median (plain lines), and quartiles (dashed lines) are indicated for each monthly distribution.

### 3.3. Synoptic Conditions Driving Snowfall

While most of the precipitation falls on the coastal areas of Antarctica, occasional poleward flow brings moisture to continental sites. Figure 4 shows the 500-hPa geopotential height anomaly relative to the seasonal average (30-day rolling mean of the climatology calculated on 1979–2015), for the days with high snowfall at ABN. Large precipitation events ( $\text{SMB} > 1 \text{ mm day}^{-1}$ ) on the East Antarctic Plateau are consistently associated with positive geopotential height anomalies corresponding to high pressure over Wilkes Land and Adélie Land (located in  $60\text{--}75^\circ\text{S}$ ,  $120\text{--}150^\circ\text{E}$ ), northeast of ABN. These high-pressure anomalies channel warm and moist air inland, causing the precipitation.

The influence of blocking on snowfall has been shown for Dome C, where high-pressure anomalies forces air masses inland from the Indian Ocean (Scarchilli et al., 2011). The blocking is located at lower latitudes and funnels the air masses from the Indian Ocean over the East Antarctic Plateau. We therefore expect blocking events to have a regional footprint on the plateau, as the moisture precipitates along the air mass transport path when it moves inland, up the plateau slope, and cools down (see Figure S12, temporal correlation maps of daily SMB and temperatures). Although the spatial representativeness of ABN is limited to a few hundreds of kilometers, the mechanisms involved in high-precipitation events are consistent across the East Antarctic Plateau at comparable altitudes and therefore responsible for a similar part of interannual variability (Turner et al., 2019). Schlosser et al. (2010) also showed that a few synoptic events were responsible for most of the precipitation at Kohonen Station, another East Antarctic Plateau site. Consequently, the findings at ABN site may be valid for other regions of Antarctica.

To assess the influence of blocking on precipitation at ABN, a blocking index is defined in the area of high geopotential anomalies associated with precipitation (Figure 4a, yellow box): the index is the ratio of grid points with a 500-hPa geopotential height anomaly larger than  $+100 \text{ m}$  lasting for at least 5 days in the  $60\text{--}70^\circ\text{S}$ ,  $120\text{--}150^\circ\text{E}$  area (Wilkes and Adélie Coasts). The blocking index values range from 0

(no blocking: no grid point with persistent  $+100\text{-m}$  geopotential anomaly) to 1 (all grid points with a blocking). This ratio is defined daily, taking the past 5 days for the computation, and is averaged to monthly resolution. There is a positive correlation of the blocking with monthly snowfall at ABN ( $r = 0.37$ ,  $p$  value  $< 0.01$ ), which supports the role of blocking in East Antarctic precipitations.

In the Southern Hemisphere, the prevalent atmospheric modes are the Baroclinic Annular Mode (BAM) and the Southern Annular Mode (SAM), which are defined as the first empirical orthogonal functions of eddy kinetic energy and atmospheric surface pressure, respectively, between  $20^\circ\text{S}$  and  $70^\circ\text{S}$  (Marshall & Thompson, 2016). BAM and SAM both influence Antarctic precipitation (Marshall et al., 2017): BAM positive phases are associated with an enhanced poleward moisture flux and thus result in increased precipitation in most of Antarctica. On the other hand, SAM positive phases imply a strong latitudinal gradient of atmospheric pressures that enhances zonal flow and prevents blockings that favor moisture transport to inland Antarctica and result in reduced precipitation on East Antarctic Plateau. These patterns are observed year-round but are weakest in austral summer. The annual SAM Marshall index (Marshall, 2003) is indeed negatively correlated with the blocking index ( $r = -0.77$ ) and annual precipitations at ABN ( $r = -0.35$ ) from 1979 to 2015. Because the SAM is responsible for most of the variability in the Southern Hemisphere and because it is a zonal feature, changes in precipitation and temperature associated with SAM affect homogeneously most of the East Antarctic Plateau at longer timescales, which explains why SMB and temperature at

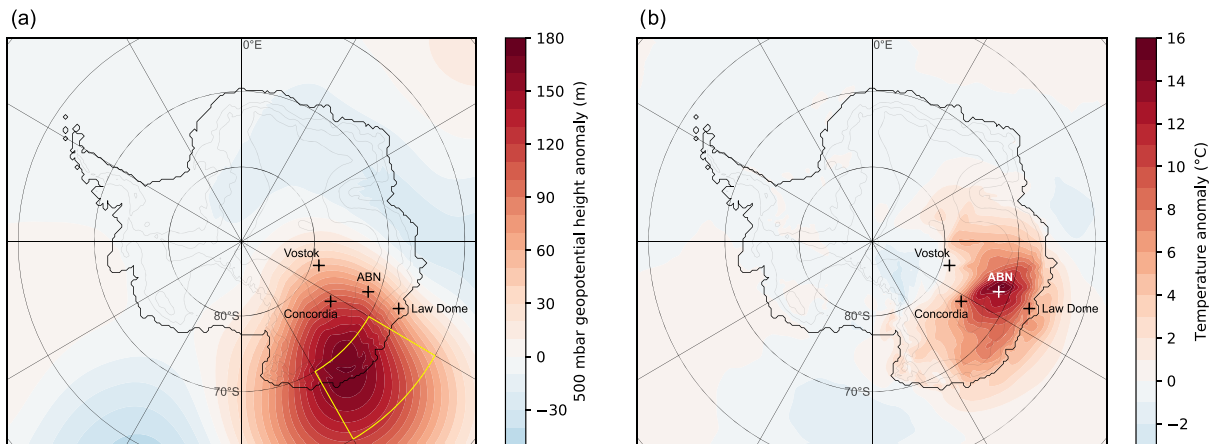


**Figure 4.** (a) Mean 500-hPa geopotential height anomaly and (b) mean 2-m temperature anomaly, when daily SMB at ABN is larger than 1 mm w.eq. day<sup>-1</sup> (1,217 days on a total of 13,514, on the 1979–2015 period). We define a blocking index for the region in the yellow box as a geopotential height anomaly greater than 100 m lasting for at least 5 days (see text for detail on computation).

ABN are positively correlated with a large part of the plateau at annual resolution (Figure S13). The precipitation at inland East Antarctica responds to large-scale atmospheric patterns via the blocking over the coast.

### 3.4. Temperature Anomaly Associated With Precipitation Events

As we have shown, large precipitation events are associated with meridional airflow, due to a high-pressure system forcing oceanic air masses inland. In this section, we quantify the temperature anomalies induced by the specific atmospheric conditions during snowfall.

Air masses forced inland cause a warming of air temperature at ABN, both due to the advection of air from the warmer ocean and due to the latent heat released by condensation. Moreover, the pressure dipole counters the usual surface winds from south to north and breaks the temperature inversion that is settled especially in winter months. By comparing surface temperatures, we would see both warm air intrusion and breaking of temperature inversion. In order to focus only on the air temperature at which condensation happens, we hereafter discuss the temperatures at a vertical level where pressure is 90% of surface pressure ( $P_{90}$ ), which is above inversion year-round (Figure S15); thus, more representative of the condensation level at which isotopic signal is acquired (Jouzel & Merlivat, 1984).

We compare the probability of density functions of monthly mean temperatures, with monthly snowfall-weighted mean temperatures (Figure 5). The latter are representative of the temperature of snowy days weighted for the amount of precipitation each day, as would be recorded in snow isotopes in ideal conditions, ignoring postdeposition effects. Monthly snowfall-weighted mean temperature ( $m_w$ ) is defined as the mean of daily temperatures ( $T_{\text{day}}$ ) weighted by the snowfall ( $P_{\text{day}}$ ) on the corresponding day:

$$m_w = \frac{\sum_{\text{day}=1}^{31} T_{\text{day}} * P_{\text{day}}}{\sum_{\text{day}=1}^{31} P_{\text{day}}}$$

Monthly mean temperatures (white, nonweighted) are characterized by an average of  $-24 \pm 4^\circ\text{C}$  in December and January. In winter, the monthly mean temperatures decrease to  $-33 \pm 5^\circ\text{C}$ . The interquartile range is lower in summer ( $\sim 2^\circ\text{C}$  in DJ) than in winter ( $\sim 3^\circ\text{C}$  in MJJA). Interquartile ranges are slightly larger ( $+0.4^\circ\text{C}$ ) for snowfall-weighted monthly means, and they also evidence a greater variability in the winter months with interquartile ranges up to  $4.1^\circ\text{C}$ . The monthly snowfall-weighted temperatures (blue) are warmer than mean temperatures (white) of the corresponding month by an average difference of  $+1.82^\circ\text{C}$ , because large precipitations coincide with warm temperature anomalies (a 1-year time series of temperature and precipitation illustrates this in Figure S16). However, months with higher SMB have a significantly larger temperature bias, so the snowfall-weighted difference increases to  $+2.83^\circ\text{C}$  when accounting for the

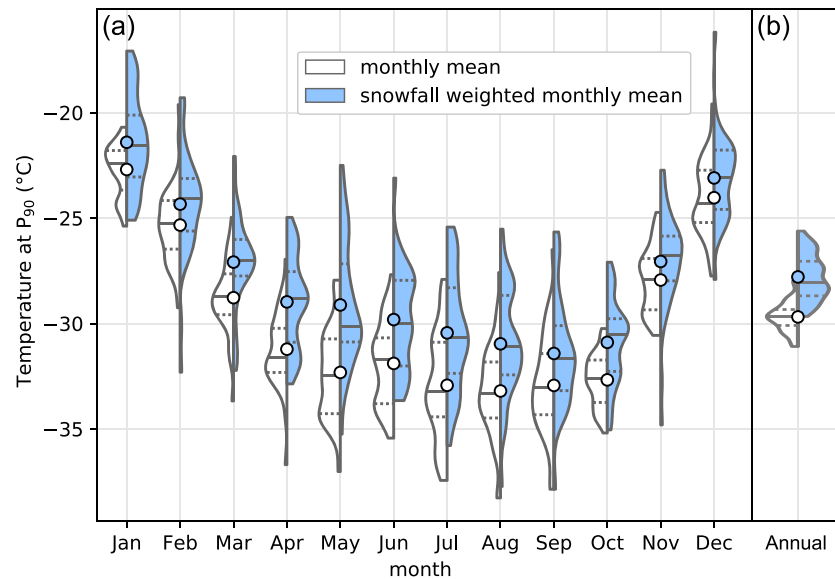


**Figure 5.** (a) Probability density function of monthly mean temperatures (white) and snowfall-weighted mean temperatures (blue). Mean (colored circles), median (plain lines), and quartiles (dashed lines) are indicated for each month distribution.  $P_{90}$  refers to the vertical level where pressure equals 90% of the surface pressure and is above inversion year-round. (b) Same as (a) but for annual temperatures distribution.

snowfall of each month relative to the total snowfall of the study period (1979–2015). Combined with the cold bias due to the seasonality of precipitation of  $-0.86^{\circ}\text{C}$  (given in section 3.1), the resulting bias associated with snowfall is  $+1.97^{\circ}\text{C}$  and is equivalent to the difference between the mean temperature and the snowfall-weighted mean temperature for the 1979–2015 period.

Because the continental temperatures drop very low in the winter, the arrival of precipitating warm oceanic air masses contrasts even more in the coldest months, so the warm bias is larger. Consequently, the total amplitude of the annual cycle of temperature is lowered in the precipitation-weighted mean. Increased variability in the winter dominates the average signal, so the temperature record will reflect the occurrence (or absence) of warm events in the winter months.

#### 4. Water Stable Isotopes in ECHAM5-wiso

We discussed in the previous section how snowfall coincides with temperatures warmer than average conditions. Here, we show how this bias can be transmitted to water isotopes using precipitation values from the ECHAM5-wiso model.

Figure 6 illustrates the relationship between precipitation  $\delta^{18}\text{O}$  and the daily temperature at  $P_{90}$  in the ECHAM5-wiso model at the ABN grid point. Each point also shows the daily precipitation amount on a color scale, and the linear regression was computed using the points weighted by the precipitation amount so that points with larger precipitation will have proportionally greater influence on the isotope-temperature slope, following a weighted orthogonal distance regression (Boggs et al., 1992). This method is equivalent to using monthly weighted means to compute the linear regression, but here we show the larger spread provided by daily values compared to monthly means. Additionally, we distinguish winter points in blue (May, June, July, and August) from summer points in red (December and January). We chose to limit the summer months to December and January as the temperature quickly decreases at the end of summer (as shown in Figure 5), whereas the winter months follow a more similar distribution. Scatter plots for each season can be found in Figure S17.

The temperature during precipitation events ranges from approximately  $-45^{\circ}\text{C}$  to  $-20^{\circ}\text{C}$  in winter and  $-30^{\circ}\text{C}$  to  $-10^{\circ}\text{C}$  in summer. The modeled  $\delta^{18}\text{O}$  ranges from  $-50\text{‰}$  to  $-20\text{‰}$  in summer and from  $-110\text{‰}$  to  $-25\text{‰}$  in winter, with most of the points above  $-60\text{‰}$ . Precipitation events with  $\delta^{18}\text{O}$  below  $-60\text{‰}$  have precipitation rates lower than  $0.01\text{ mm w.eq. day}^{-1}$  and therefore barely influence the total



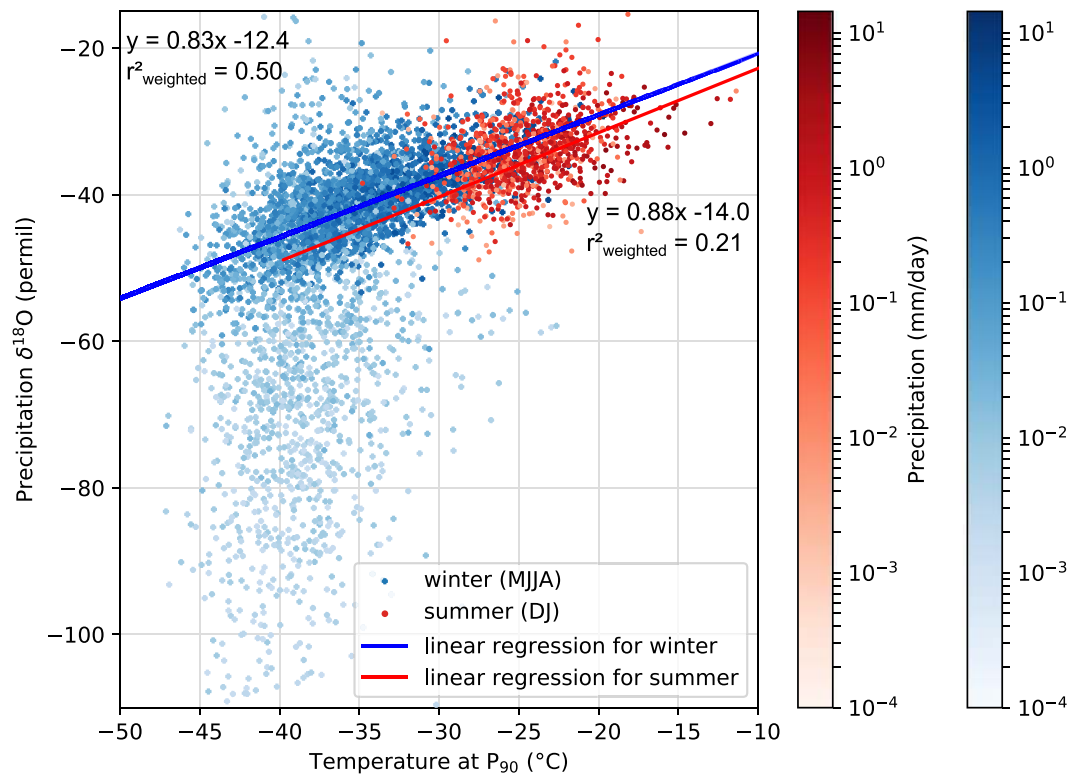


**Figure 6.** Scatter plot of daily  $\delta^{18}\text{O}$  in precipitation and temperature at  $P_{90}$  at the ABN grid point, for summer (December–January, red) and winter (May–August, blue). The color scales indicate the daily precipitation amount. Linear regressions are computed for both summer and winter with an orthogonal distance least mean squares with each point weighted with its daily precipitation.  $P_{90}$  refers to the vertical level where pressure equals 90% of the surface pressure and is above inversion year-round. Equation of weighted regressions are indicated along with the Pearson weighted correlation coefficient (e.g., Pozzi et al., 2012).

snow  $\delta^{18}\text{O}$  record. The very depleted  $\delta^{18}\text{O}$  of low snowfall events are probably an artifact caused by the calculation of  $\delta^{18}\text{O}$  in ECHAM5-wiso, which is computed from the division of absolute quantities of  $\text{H}_2^{16}\text{O}$  and  $\text{H}_2^{18}\text{O}$  isotopologues. Despite a large spread of data points, especially in low precipitation events (lighter colors), there is a clear temperature-isotope relationship. The weighted regressions give slopes of  $0.81\text{--}0.86\text{‰ }^\circ\text{C}^{-1}$  for winter and  $0.81\text{--}0.95\text{‰ }^\circ\text{C}^{-1}$  for summer (95% confidence intervals) consistent with the  $0.84 \pm 0.05\text{‰ }^\circ\text{C}^{-1}$  slope found in precipitation  $\delta^{18}\text{O}$  over inversion temperature at Dome C (Stenni et al., 2016). The variability, both in isotopes and temperature, is larger in the winter season, but the linear regressions computed for each seasons have the same slope within the margin of error. This indicates that processes responsible for the isotopic signature in the snow are similar year-round, despite seasonal changes in moisture source and air mass transport (Sodemann & Stohl, 2009).

Changes in temperature will also affect the snow  $\delta^{18}\text{O}$ , as the temperature and  $\delta^{18}\text{O}$  are strongly correlated. Even without the low snowfall events, the high winter variability evidenced for temperature in section 3.4 is also present in  $\delta^{18}\text{O}$  and should drive the annual variability in isotopes as well. Therefore, we can use  $\delta^{18}\text{O}$  as a proxy of temperature and atmospheric conditions described in section 3.3. Additionally, the  $+1.97^\circ\text{C}$  mean bias will be translated in an approximately  $+1.7\text{‰}$  bias in  $\delta^{18}\text{O}$ .

In the next section, we compare snow pit  $\delta^{18}\text{O}$  measurements with modeled temperature (MAR) and isotopes (ECHAM), and discuss the climate features that get recorded in the  $\delta^{18}\text{O}$  record.

### 5. Comparison of Isotope Records and Climate From 2005 to 2014

Here, we compare the measurements of  $\delta^{18}\text{O}$  from samples collected from two snow pit profiles,  $\delta^{18}\text{O}$  from a shallow firn core, temperature from the MAR model,  $\delta^{18}\text{O}$  in ECHAM5-wiso model, and two atmospheric indices: the blocking index introduced in section 3.3 and the SAM Marshall index (Marshall, 2003), all

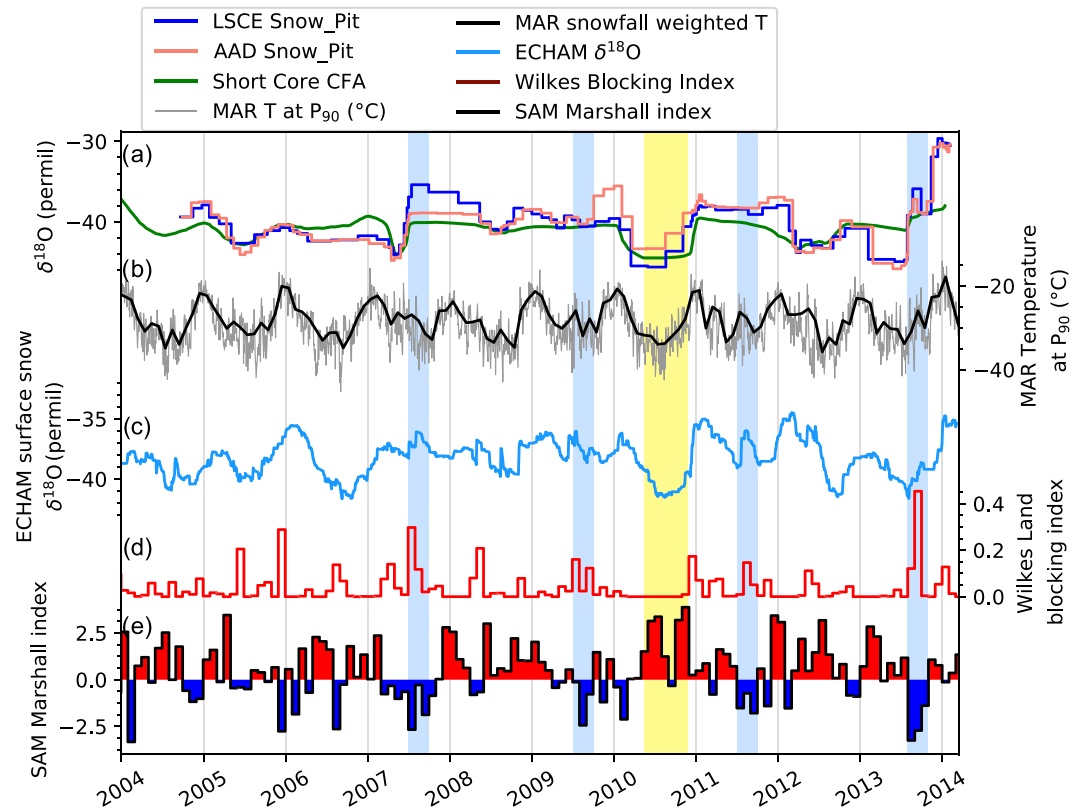


**Figure 7.** Comparison of (a) three high-resolution records: two snow pit profiles and a short core, with (b) temperature at  $P_{90}$  at daily resolution (thin gray line) and monthly snowfall-weighted mean temperature (thick black line), (c) modeled surface snow  $\delta^{18}\text{O}$  (buffer averaging the  $\delta^{18}\text{O}$  in the last 10 mm w.eq. of precipitations), (d) Wilkes Land blocking index, and (e) SAM Marshall monthly index (Marshall, 2003). Some periods with particularly negative (resp. positive) SAM index are highlighted with blue (yellow) shading.

shown in Figure 7. The surface snow  $\delta^{18}\text{O}$  parameter given by ECHAM5-wiso is a simple buffer where the  $\delta^{18}\text{O}$  of the last 10 mm w.eq. of precipitation is averaged, with respect to the quantity of precipitation. Consequently, this  $\delta^{18}\text{O}$  value is precipitation weighted. We illustrate the average in the surface snow buffer of ECHAM5-wiso in Figure S18. We describe hereafter the relationships between measured  $\delta^{18}\text{O}$ , modeled  $\delta^{18}\text{O}$ , and atmospheric conditions.

We give the Pearson correlation coefficients of the different series in Figure 8: the correlation for annually averaged (Figure 8b) series are significant if they are higher than 0.67 ( $p$  value < 0.05). Dating uncertainties and low interannual variabilities over a period as short as 9 years should call for caution when interpreting the statistics computed on annual averages. The seasonal signal drives the correlation for non-averaged series (Figure 8a), and there might be autocorrelation within series.

The two snow pit records have near-identical  $\delta^{18}\text{O}$  content ( $r = 0.95$ ), because the samples were taken with similar resolution (2.5 cm for AAD and 3 cm for LSCE) at 1-m distance from each other. The short core  $\delta^{18}\text{O}$  also shows similar features with a good correlation with both snow pit measurements ( $r = 0.72$  and  $r = 0.65$ ) but significantly lower than between the two snow pits. The lower correlation value might be due to (1) the smoothing of high frequencies caused by the CFA technique used to measure this core (Gkinis et al., 2011; Holme et al., 2018) and/or (2) difference in snow deposition, as the short core was taken  $\sim 200$  m away from the snow pits. Snow at low-accumulation plateau sites exchanges isotopes with underlying snow through diffusion (Casado et al., 2018) and can be deposited in patches inducing differences in layer thicknesses related to surface roughness (Picard et al., 2019). These processes increase horizontal variability and influence the mean  $\delta^{18}\text{O}$ . Münch et al. (2016) also show that stratigraphic noise lowers the correlation of two  $\delta^{18}\text{O}$  series in a few meters at Kohlen Station in Dronning Maud Land (dropping from  $r = 1.0$  to  $r = 0.5$

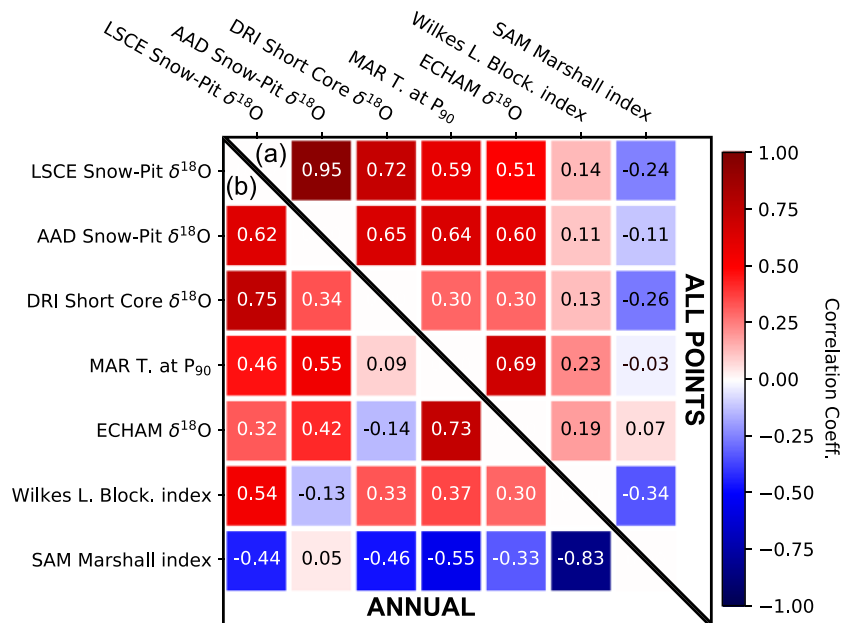


**Figure 8.** Pearson correlation coefficients table between the series shown in Figure 7: snow pits measured at LSCE and AAD, short core measured at DRI, MAR-modeled temperature at  $P_{90}$ , ECHAM5-wiso modeled surface snow  $\delta^{18}\text{O}$  (buffer averaging the  $\delta^{18}\text{O}$  in the last 10 mm w.eq. of precipitations), Wilkes Land blocking index, and SAM Marshall monthly index. Correlations are shown for (a) the maximum resolution signal (all series were resampled on LSCE snow pit resolution, with an average of 8 points year<sup>-1</sup>) and (b) the annually averaged signal.

in 10 m, then plateauing at 0.5 correlation), albeit the accumulation at Kohnen Station (64 mm w.eq. year<sup>-1</sup>) is lower than at ABN (119 mm w.eq. year<sup>-1</sup>), so the ABN records show higher correlations (minimum  $r = 0.65$ ) and will better record the decadal climate signal than plateau sites with lower accumulation. The high spatial variability is further evidenced by the large differences in annual accumulation between the three snow records (Table S1). An approach to overcome spatial variability, and increase signal to noise ratio, is to stack multiple records (e.g., Graf et al., 2002). In our case, stacking the three  $\delta^{18}\text{O}$  records (Figures S19 and S20) did not improve our understanding of how the climate signal is recorded in the snow. More studies would be needed to quantify the variability of the lower East Antarctic Plateau. Despite the uncertainties,  $\delta^{18}\text{O}$  of all three snow records show large changes within a single winter season, from  $-45\text{‰}$  to  $-35\text{‰}$  (e.g., 2007 or 2013), highlighting the large variability of winter signals.

The modeled temperatures from MAR and modeled  $\delta^{18}\text{O}$  from ECHAM5-wiso, which are in good agreement ( $r = 0.69$  for the period 2005–2014), both show positive correlations with snow pit  $\delta^{18}\text{O}$  at subannual resolution ( $r = 0.51$ – $0.64$ ), although the correlation is slightly lower with the DRI short core ( $r = 0.30$ ). The absence of surface and postdeposition processes in ECHAM5-wiso, which basically gives the precipitation  $\delta^{18}\text{O}$ , may partly explain why the modeled  $\delta^{18}\text{O}$  is not better correlated to measured  $\delta^{18}\text{O}$  than the modeled temperature is. ECHAM5-wiso or other isotope-enabled atmospheric models would highly benefit from being coupled with glaciological models that account for surface and postdeposition processes to give a range of values comparable to  $\delta^{18}\text{O}$  recorded in ice cores, within a confidence interval. The standard deviation of interpolated ECHAM5-wiso  $\delta^{18}\text{O}$  values is twice as large as the standard deviation of  $\delta^{18}\text{O}$  measured in snow pits, due to the overestimation of  $\delta^{18}\text{O}$  variability in the model, and lack of smoothing from postdepositional processes. Despite the different amplitude, the  $\delta^{18}\text{O}$  measurements and modeled  $\delta^{18}\text{O}$  exhibit strong consistent signals especially in the winters 2007, 2009, 2010, 2011, and 2013 that are related to temperature anomalies (Figure 7, shaded in blue and yellow), arguing that atmospheric signals remain after postdeposition.

As shown in section 3.3, a blocking in the Wilkes and Adélie Land favors the meridional transport of moisture and warmth inland East Antarctica; thus, the blocking index is moderately positively correlated with most  $\delta^{18}\text{O}$  records and temperature at ABN ( $r = 0.11$ – $0.23$ , Figure 8a). The SAM, which enhances zonal

flow in its positive phase, isolates the Antarctic continent and reduces the probability of blocking (Parsons et al., 2016), which explains why its index is negatively correlated with annual temperature ( $r = -0.55$ ) and  $\delta^{18}\text{O}$  ( $r = -0.33$  with ECHAM  $\delta^{18}\text{O}$ ) at ABN on annual means.

We highlight in Figure 7 some remarkable positive (yellow shading) and negative (blue shading) phases of SAM that occurred during winter or spring. Extended positive SAM phase such as the winter 2010 prevents the intrusion of marine air masses, so the average winter temperature and isotopic signals remain very low. On the other hand, intense negative SAM phases allow for strong blocking and thus warm anomalies at ABN and high  $\delta^{18}\text{O}$  values. For example, the winter  $\delta^{18}\text{O}$  in 2011 in snow pit records is almost as high as previous and following summers. This relationship between SAM and isotopes at ABN is however not valid for every year, because it depends on (1) persistent conditions throughout a season, (2) the occurrence of precipitation to capture the anomaly in  $\delta^{18}\text{O}$  that is all the more unlikely given that SAM positive phases prevent snowfall, and (3) other atmospheric patterns may play a role, especially since SAM is defined at a hemispheric scale and is poorly suited to describe the meridional flow at a specific longitude. The multiyear average temperature signal is driven by the winter variability. The average will depend primarily on the frequency and intensity of high-precipitation events; atmospheric modes (SAM or other Indian Ocean-centered EOFs) play an important role in the control in the occurrence of such events on long timescales.

The recent trend in SAM, with a strengthening of positive phases (Marshall, 2004), may prevent the coastal blockings necessary to channel precipitating systems inland East Antarctica. This trend, associated with global warming and poleward shifts of atmospheric circulation, may induce a lowering in apparent temperatures on the plateau, by reducing the number and intensity of warm precipitation events reaching the high-altitude sites. This could explain why no significant warming has been observed yet on East Antarctic Plateau (Marshall, 2007; Stenni et al., 2017). The study of isotopes in the ABN ice core will help clarify the recent trend on the lower part of the East Antarctic Plateau between 110°E and 140°E.

## 6. Conclusion

We used the regional model MAR and isotope-enabled model ECHAM5-wiso to study the processes associated with precipitation at East Antarctic site ABN and their potential effect on water isotopes, which are commonly used as a temperature proxy in ice cores. The accumulation at ABN is higher than other ice-core drilling sites at higher elevations on the East Antarctic Plateau, which makes it an excellent candidate for studying recent climate variability of this region at decadal to centennial scale. We showed that precipitation events with daily SMB higher than 1 mm w.eq. day<sup>-1</sup> are of particular importance given that they account for 58% of total SMB at ABN. These events are responsible for the interannual variability of SMB, temperature, and isotopes. The occurrence of high-precipitation events at ABN coincides with the presence of high pressures on Wilkes Land that channels warm and moist air inland East Antarctica, causing warm anomalies compared to the seasonal mean. The temperature biases from seasonality of precipitations ( $-0.86^\circ\text{C}$ ) and warm events bringing precipitations ( $+2.83^\circ\text{C}$ ) result in a mean bias of  $+1.97^\circ\text{C}$ .

Because of larger variability in both isotopes and temperature during the winter season, the interannual signal will depend primarily on the winter conditions, which in turn depend on whether synoptic events can reach the plateau or not. The blocking favoring precipitation at ABN is themselves conditioned by atmospheric circulation patterns and is more likely to happen with a negative phase of the SAM. The results presented for ABN may apply for other sites, because mechanisms responsible for high-precipitation events are comparable across the East Antarctic Plateau.

As isotopes reflect temperature changes, we can use the isotopes in ice core to trace past changes in atmosphere circulation conditions. Over the short timescale presented here, different series of  $\delta^{18}\text{O}$  from snow pits and a short core clearly record large anomalies in SAM and atmospheric blocking happening in the winter, which supports the use of  $\delta^{18}\text{O}$  (or its equivalent) as a tracer of atmospheric circulation in East Antarctic Plateau ice cores, at annual to decadal scale.

## Data Availability Statement

ERA-Interim was used for forcing the models and is available for registered users at Copernicus. The last version of MAR is freely distributed at <http://mar.cnrs.fr/>. ECHAM source code is freely available to the public,

and model outputs can be found at <http://cera-www.dkrz.de>. Snow isotope data, age models, density profiles, and accumulation estimates are accessible online at [data.aad.gov.au/metadata/records/AAS\\_4075\\_ABN1314\\_Glacial\\_isotopic\\_composition](http://data.aad.gov.au/metadata/records/AAS_4075_ABN1314_Glacial_isotopic_composition).

### Acknowledgments

This work was supported by LEFE project ABN-2k, the project Antarctic-SNOW from the Foundation Albert 2 de Monaco (FA2M), the Australian Antarctic Division (AAS 4075), and the Australian Government's Cooperative Research Centres Programme through the Antarctic Climate and Ecosystems Cooperative Research Centre (ACE CRC). The research leading to these results has received funding from the European Research Council under the European Union's Seventh Framework Programme (FP7/2007-2013)/RC Grant Agreement 306045. We are grateful to Olivia Maselli, Christopher Plummer, and Mana Inoue for their help on field for digging the snow pit and to Tas Van Ommen for the density measurements. We thank an anonymous reviewer for constructive comments on the manuscript.

### References

- Agosta, C., Amory, C., Kittel, C., Orsi, A., Favier, V., Gallée, H., et al. (2019). Estimation of the Antarctic surface mass balance using the regional climate model MAR (1979–2015) and identification of dominant processes. *The Cryosphere*, *13*(1), 281–296. <https://doi.org/10.5194/tc-13-281-2019>
- Altnau, S., Schlosser, E., Isaksson, E., & Divine, D. (2015). Climatic signals from 76 shallow firn cores in Dronning Maud Land, East Antarctica. *The Cryosphere*, *9*(3), 925–944. <https://doi.org/10.5194/tc-9-925-2015>
- Bertler, N. A. N., Mayewski, P. A., & Carter, L. (2011). Cold conditions in Antarctica during the Little Ice Age—Implications for abrupt climate change mechanisms. *Earth and Planetary Science Letters*, *308*(1–2), 41–51. <https://doi.org/10.1016/j.epsl.2011.05.021>
- Bertler, N. A. N., Conway, H., Dahl-Jensen, D., Emanuelsson, D. B., Winstrup, M., Vallenga, P. T., et al. (2018). The Ross Sea Dipole—Temperature, snow accumulation and sea ice variability in the Ross Sea region, Antarctica, over the past 2700 years. *Climate of the Past*, *14*(2), 193–214. <https://doi.org/10.5194/cp-14-193-2018>
- Boggs, P. T., Byrd, R. H., Rogers, J. E., & Schnabel, R. B. (1992). User's reference guide for odrpack version 2.01: Software for weighted orthogonal distance regression. <https://doi.org/10.6028/NIST.IR.4834>
- Casado, M., Landais, A., Picard, G., Münch, T., Laepple, T., Stenni, B., et al. (2018). Archival processes of the water stable isotope signal in East Antarctic ice cores. *The Cryosphere*, *12*(5), 1745–1766. <https://doi.org/10.5194/tc-12-1745-2018>
- Casado, M., Münch, T., & Laepple, T. (2019). Climatic information archived in ice cores: impact of intermittency and diffusion on the recorded isotopic signal in Antarctica [preprint]. *Climate of the Past*. <https://doi.org/10.5194/cp-2019-134>
- Cole-Dai, J., & Mosley-Thompson, E. (1999). The Pinatubo eruption in south pole snow and its potential value to ice-core paleovolcanic records. *Annals of Glaciology*, *29*, 99–105. <https://doi.org/10.3189/172756499781821319>
- Craig, H. (1961). Isotopic variations in meteoric waters. *Science, New Series*, *133*(3465), 1702–1703.
- Dansgaard, W. (1964). Stable isotopes in precipitation. *Tellus*, *16*(4), 436–468. <https://doi.org/10.1111/j.2153-3490.1964.tb00181.x>
- Dee, D. P., Uppala, S. M., Simmons, A. J., Berrisford, P., Poli, P., Kobayashi, S., et al. (2011). The ERA-Interim reanalysis: Configuration and performance of the data assimilation system. *Quarterly Journal of the Royal Meteorological Society*, *137*(656), 553–597. <https://doi.org/10.1002/qj.828>
- Ekaykin, A. A., Vladimirova, D. O., Lipenkov, V. Y., & Masson-Delmotte, V. (2017). Climatic variability in Princess Elizabeth Land (East Antarctica) over the last 350 years. *Climate of the Past*, *13*(1), 61–71. <https://doi.org/10.5194/cp-13-61-2017>
- EPICA community members (2004). Eight glacial cycles from an Antarctic ice core. *Nature*, *429*(6992), 623–628. <https://doi.org/10.1038/nature02599>
- Fogt, R. L., Goergens, C. A., Jones, J. M., Schneider, D. P., Nicolas, J. P., Bromwich, D. H., & Dusselier, H. E. (2017). A twentieth century perspective on summer Antarctic pressure change and variability and contributions from tropical SSTs and ozone depletion. *Geophysical Research Letters*, *44*, 9918–9927. <https://doi.org/10.1002/2017GL075079>
- Fréville, H., Brun, E., Picard, G., Tatarinova, N., Arnaud, L., Lanconelli, C., et al. (2014). Using MODIS land surface temperatures and the Crocus snow model to understand the warm bias of ERA-Interim reanalyses at the surface in Antarctica. *The Cryosphere*, *8*(4), 1361–1373. <https://doi.org/10.5194/tc-8-1361-2014>
- Gallée, H., Preunkert, S., Argenti, S., Frey, M. M., Genthon, C., Jourdain, B., et al. (2015). Characterization of the boundary layer at Dome C (East Antarctica) during the OPAL summer campaign. *Atmospheric Chemistry and Physics*, *15*(11), 6225–6236. <https://doi.org/10.5194/acp-15-6225-2015>
- Gkinis, V., Popp, T. J., Blunier, T., Bigler, M., Schüpbach, S., Kettner, E., & Johnsen, S. J. (2011). Water isotopic ratios from a continuously melted ice core sample. *Atmospheric Measurement Techniques*, *4*(11), 2531–2542. <https://doi.org/10.5194/amt-4-2531-2011>
- Goursaud, S., Masson-Delmotte, V., Favier, V., Orsi, A., & Werner, M. (2018). Water stable isotope spatio-temporal variability in Antarctica in 1960–2013: Observations and simulations from the ECHAM5-wiso atmospheric general circulation model. *Climate of the Past*, *14*(6), 923–946. <https://doi.org/10.5194/cp-14-923-2018>
- Graf, W., Oerter, H., Reinwarth, O., Stichler, W., Wilhelms, F., Miller, H., & Mulvaney, R. (2002). Stable-isotope records from Dronning Maud Land, Antarctica. *Annals of Glaciology*, *35*, 195–201. <https://doi.org/10.3189/172756402781816492>
- Gupta, P., Noone, D., Galewsky, J., Sweeney, C., & Vaughn, B. H. (2009). Demonstration of high-precision continuous measurements of water vapor isotopologues in laboratory and remote field deployments using wavelength-scanned cavity ring-down spectroscopy (WS-CRDS) technology. *Rapid Communications in Mass Spectrometry*, *23*(16), 2534–2542. <https://doi.org/10.1002/rcm.4100>
- Holme, C., Gkinis, V., & Vinther, B. M. (2018). Molecular diffusion of stable water isotopes in polar firn as a proxy for past temperatures. *Geochimica et Cosmochimica Acta*, *225*, 128–145. <https://doi.org/10.1016/j.gca.2018.01.015>
- Jones, J. M., Gille, S. T., Goosse, H., Abram, N. J., Canziani, P. O., Charman, D. J., et al. (2016). Assessing recent trends in high-latitude Southern Hemisphere surface climate. *Nature Climate Change*, *6*(10), 917–926. <https://doi.org/10.1038/nclimate3103>
- Jouzel, J. (2003). Magnitude of isotope/temperature scaling for interpretation of central Antarctic ice cores. *Journal of Geophysical Research*, *108*(D12), 4361. <https://doi.org/10.1029/2002JD002677>
- Jouzel, J., & Merlivat, L. (1984). Deuterium and oxygen 18 in precipitation: Modeling of the isotopic effects during snow formation. *Journal of Geophysical Research*, *89*(D7), 11749. <https://doi.org/10.1029/JD089iD07p11749>
- Marshall, G. J. (2003). Trends in the Southern Annular Mode from observations and reanalyses. *Journal of Climate*, *16*(24), 4134–4143. [https://doi.org/10.1175/1520-0442\(2003\)016<4134:TITSAM>2.0.CO;2](https://doi.org/10.1175/1520-0442(2003)016<4134:TITSAM>2.0.CO;2)
- Marshall, G. J. (2004). Causes of exceptional atmospheric circulation changes in the Southern Hemisphere. *Geophysical Research Letters*, *31*, L14205. <https://doi.org/10.1029/2004GL019952>
- Marshall, G. J. (2007). Half-century seasonal relationships between the southern annular mode and Antarctic temperatures. *International Journal of Climatology*, *27*(3), 373–383. <https://doi.org/10.1002/joc.1407>
- Marshall, G. J., & Thompson, D. W. J. (2016). The signatures of large-scale patterns of atmospheric variability in Antarctic surface temperatures: Antarctic temperatures. *Journal of Geophysical Research: Atmospheres*, *121*, 3276–3289. <https://doi.org/10.1002/2015JD024665>
- Marshall, G. J., Thompson, D. W. J., & Broeke, M. R. (2017). The signature of Southern Hemisphere atmospheric circulation patterns in Antarctic precipitation. *Geophysical Research Letters*, *44*, 11,580–11,589. <https://doi.org/10.1002/2017GL075998>



- Maselli, O. J., Fritzsche, D., Layman, L., McConnell, J. R., & Meyer, H. (2013). Comparison of water isotope-ratio determinations using two cavity ring-down instruments and classical mass spectrometry in continuous ice-core analysis. *Isotopes in Environmental and Health Studies*, *49*(3), 387–398. <https://doi.org/10.1080/10256016.2013.781598>
- Masson-Delmotte, V., Hou, S., Ekaykin, A., Jouzel, J., Aristarain, A., Bernardo, R. T., et al. (2008). A review of Antarctic surface snow isotopic composition: Observations, atmospheric circulation, and isotopic modeling. *Journal of Climate*, *21*(13), 3359–3387. <https://doi.org/10.1175/2007JCLI2139.1>
- McConnell, J. R., Lamorey, G. W., Lambert, S. W., & Taylor, K. C. (2002). Continuous ice-core chemical analyses using inductively coupled plasma mass spectrometry. *Environmental Science & Technology*, *36*(1), 7–11. <https://doi.org/10.1021/es011088z>
- Münch, T., Kipfstuhl, S., Freitag, J., Meyer, H., & Laepple, T. (2016). Regional climate signal vs. local noise: A two-dimensional view of water isotopes in Antarctic firn at Kohnen Station, Dronning Maud Land. *Climate of the Past*, *12*, 1565–1581. <https://doi.org/10.5194/cp-12-1565-2016>
- Parsons, S., Renwick, J. A., & McDonald, A. J. (2016). An assessment of future Southern Hemisphere blocking using CMIP5 projections from four GCMs. *Journal of Climate*, *29*(21), 7599–7611. <https://doi.org/10.1175/JCLI-D-15-0754.1>
- Persson, A., Langen, P. L., Ditlevsen, P., & Vinther, B. M. (2011). The influence of precipitation weighting on interannual variability of stable water isotopes in Greenland. *Journal of Geophysical Research*, *116*, D20120. <https://doi.org/10.1029/2010JD015517>
- Picard, G., Arnaud, L., Caneill, R., Lefebvre, E., & Lamare, M. (2019). Observation of the process of snow accumulation on the Antarctic Plateau by time lapse laser scanning. *The Cryosphere*, *13*(7), 1983–1999. <https://doi.org/10.5194/tc-13-1983-2019>
- Pozzi, F., di Matteo, T., & Aste, T. (2012). Exponential smoothing weighted correlations. *The European Physical Journal B*, *85*(6), 1–21. <https://doi.org/10.1140/epjb/e2012-20697-x>
- Rhodes, R. H., Bertler, N. A. N., Baker, J. A., Steen-Larsen, H. C., Sneed, S. B., Morgenstern, U., & Johnsen, S. J. (2012). Little ice age climate and oceanic conditions of the Ross Sea, Antarctica from a coastal ice core record. *Climate of the Past*, *8*(4), 1223–1238. <https://doi.org/10.5194/cp-8-1223-2012>
- Scarchilli, C., Frezzotti, M., & Ruti, P. M. (2011). Snow precipitation at four ice core sites in East Antarctica: Provenance, seasonality and blocking factors. *Climate Dynamics*, *37*(9–10), 2107–2125. <https://doi.org/10.1007/s00382-010-0946-4>
- Schlosser, E., Manning, K. W., Powers, J. G., Duda, M. G., Birnbaum, G., & Fujita, K. (2010). Characteristics of high-precipitation events in Dronning Maud Land, Antarctica. *Journal of Geophysical Research*, *115*, D14107. <https://doi.org/10.1029/2009JD013410>
- Sigl, M., Fudge, T., Winstrup, M., Cole-Dai, J., Ferris, D., McConnell, J., et al. (2016). The WAIS divide deep ice core WD2014 chronology—Part 2: Annual-layer counting (0–31 ka BP). *Climate of the Past*, *19*. <https://doi.org/10.1029/2009GL040242>
- Sodemann, H., & Stohl, A. (2009). Asymmetries in the moisture origin of Antarctic precipitation. *Geophysical Research Letters*, *36*, L22803. <https://doi.org/10.1029/2009GL040242>
- Stenni, B., Curran, M. A. J., Abram, N. J., Orsi, A., Goursaud, S., Masson-Delmotte, V., et al. (2017). Antarctic climate variability on regional and continental scales over the last 2000 years. *Climate of the Past*, *13*(11), 1609–1634. <https://doi.org/10.5194/cp-13-1609-2017>
- Stenni, B., Scarchilli, C., Masson-Delmotte, V., Schlosser, E., Ciardini, V., Dreossi, G., et al. (2016). Three-year monitoring of stable isotopes of precipitation at Concordia Station, East Antarctica. *The Cryosphere*, *10*(5), 2415–2428. <https://doi.org/10.5194/tc-10-2415-2016>
- Thomas, E. R., Allen, C. S., Etourneau, J., King, A. C. F., Severi, M., Winton, V. H. L., et al. (2019). Antarctic sea ice proxies from marine and ice core archives suitable for reconstructing sea ice over the past 2000 years. *Geosciences*, *9*(12), 506. <https://doi.org/10.3390/geosciences9120506>
- Turner, J., Phillips, T., Thamban, M., Rahaman, W., Marshall, G. J., Wille, J. D., et al. (2019). The dominant role of extreme precipitation events in Antarctic snowfall variability. *Geophysical Research Letters*, *46*, 3502–3511. <https://doi.org/10.1029/2018GL081517>
- Werner, M., Langebroek, P. M., Carlsen, T., Herold, M., & Lohmann, G. (2011). Stable water isotopes in the ECHAM5 general circulation model: Toward high-resolution isotope modeling on a global scale. *Journal of Geophysical Research*, *116*, D15109. <https://doi.org/10.1029/2011JD015681>